R-05-29

An analytic method for estimating the probability of canister/fracture intersections in a KBS-3 repository

Allan Hedin
Svensk Kärnbränslehantering AB

May 2005

Svensk Kärnbränslehantering AB
Swedish Nuclear Fuel
and Waste Management Co
Box 5864
SE-102 40 Stockholm Sweden
Tel 08-459 84 00
+46 8 459 84 00
Fax 08-661 57 19
+46 8 661 57 19

ISSN 1402-3091
SKB Rapport R-05-29

An analytic method for estimating the probability of canister/fracture intersections in a KBS-3 repository

Allan Hedin
Svensk Kärnbränslehantering AB

May 2005

Contents

1 Introduction

In the KBS-3 method for final storage of spent nuclear fuel, copper canisters with a cast iron insert containing the fuel are surrounded by bentonite clay and deposited at approximately 500 m depth in saturated, granitic rock.

The fractures within the host rock, and their properties, are crucial in the evaluation of long-term safety of this storage concept. Part of the fracture population offers pathways for groundwater transport of canister corroding agents and of radionuclides, should a release from the repository occur. The fractures are also essential in the evaluation of the mechanical stability of the host rock over the, typically, one million year time scale covered by a safety assessment.

A particular problem concerns the possibility of shear movements along fractures intersecting deposition holes. Such movements, if sufficiently large, could possibly cause canister damage and hence release of radionuclides. Shear movements along fractures intersecting deposition holes may be triggered by an earthquake located to a major deformation zone near the repository. Sweden is located in a region that is at present tectonically quiet. In a 100,000 year perspective, major climate changes with severe glaciations are, however, expected in this region. Large earthquakes of magnitudes that could cause the above-mentioned effects could occur in particular in conjunction with the retreat of a major glacier /SKB, 2004/.

According to a methodology proposed in /SKB, 2004/ and in more detail in /Munier and Hökmark, 2004/, canisters should therefore not be emplaced in the immediate vicinity of major deformation zones. Additionally, canister deposition holes should not be intersected by fractures exceeding a certain size in order to avoid the possibility of shear movements larger than typically 0.1 m, which has been demonstrated to provide a reasonable margin for canister failure /Börgesson et al. 2004/.

At the present, surface based, site investigation stage, knowledge about the properties of fractures that could intersect deposition holes is only available in a statistical sense, and this will also be the case for parts of the fully excavated repository. Since full knowledge will never be possible, there will always be a residual probability that a deposition hole will be intersected by too large a fracture, despite application of appropriate selection criteria at deposition.

This report provides a method for calculating the probability of a canister location being intersected by a fracture exceeding a prescribed size, assuming that such fractures are not detected and avoided when canisters are deposited. The method is based on analytic considerations and results in analytic expressions that allow immediate calculation of the mentioned probabilities, provided that the distributions of fracture sizes and orientations are expressed in the forms treated in this report. These forms agree with those reported in the site descriptions emerging from SKB's investigations of candidate sites for a deep repository /SKB, 2004/. It is also demonstrated how the same results can be obtained through simulations. The simulation methodology can readily be extended to encompass also other types of distributions.

The purpose of this work is not to discuss or evaluate the validity of the particular models of fracture distributions used as worked examples in the report. Rather, the results point to some important features of these models from the point of view of critical fracture intersections at deposition holes. These properties need to be carefully evaluated when the safety of a site is assessed.

Chapter 2 describes the analytic model and gives an example application of the method. In chapter 3, the sensitivity of the model results to a number of input parameters is explored. Chapter 4 describes how the problem can also be numerically simulated and it is demonstrated that the simulation model yields mean results in agreement with the analytic model, as expected. Conclusions are summarised in chapter 5 and quality assurance aspects are briefly discussed in chapter 6.

The author is particularly indebted to Raymond Munier, SKB, for providing necessary geologic background information, for comments on this manuscript and for many animated discussions on this matter. Also Harald Hökmark, Clay Technology AB and Johan Andersson, JA Streamflow AB have given constructive comments on this report.

2 The analytic model

The method presented below is based on the simple notion that if the distributions of fracture sizes and orientations in a host rock are known, and if a canister is emplaced randomly in that host rock, then it is possible to calculate the probability that the canister is intersected by a fracture of specified properties, in particular by a fracture that exceeds a certain size.

The method is based on the types of statistical descriptions of fracture sizes and orientations that have emerged from SKB's on-going site investigations /SKB, 2004/. The fracture population is described as several fracture sets, each with specified distributions of sizes and orientations. The distributions of sizes and orientations within a set are assumed to be uncorrelated, an important prerequisite for the method. Furthermore, all fractures are assumed to be infinitesimally thin, circular discs.

The calculation model essentially consists of two factors, of which one is related to the fracture size distribution and the other to the distribution of fracture orientations.

The fracture intensity and fracture size distribution will correspond to an average fracture area per unit volume of host rock, a P_{32}-value, expressed in units of m^2/m^3. Part of the P_{32}-value will be associated with fractures that exceed a certain size and this critical part, a, is determined for a power-law size distribution in section 2.1. For a given rock volume, V m^3, the total critical fracture area is thus equal to $a \cdot V$ m^2.

The cylindrical canisters are to be deposited with their axes oriented vertically. If a fracture of critical size is horizontal, then canister centre-points should not be positioned within half the canister height on either side of the fracture in order to avoid intersection, giving a total canister intersection zone width around a horizontal fracture equal to the canister height. The corresponding width for a vertical fracture equals the canister diameter. For a distribution of fracture orientations, a mean intersection zone width, $\langle L \rangle$ can be calculated and this is done in section 2.2.

Given the mean total critical fracture area, a, and the mean intersection zone width, $\langle L \rangle$, a mean value of the volume of rock within which canisters would intersect fractures of critical size is calculated as $a \cdot V \cdot \langle L \rangle$. The fraction of the total volume to be avoided, ε, is thus $a \cdot \langle L \rangle$. The quantity ε can thus be interpreted as the probability that a randomly emplaced canister will be intersected by too large a fracture. This is further explained and exemplified in section 2.3.

2.1 Critical fracture area

Given a discrete fracture network (DFN) model of the fracture frequency as a function of fracture size, it is possible to estimate the total fracture area to be avoided in a certain volume of host rock. In the following, this quantity, denoted by a, is derived for a power-law distributed fracture size, and, in Appendix A, for a log-normal fracture size distribution.

2.1.1 Power-law distributed fracture sizes

The probability density function of fracture sizes, $f(r)$, is often expressed as a power-law distribution:

$$f(r) = \frac{k\, r_0^k}{r^{k+1}}, \quad r_0 \le r < \infty \tag{1}$$

where r is the fracture radius, r_0 is the smallest fracture radius considered in the model and k is a dimensionless model parameter. Each fracture set is characterised by specified values of k and r_0. To be able to calculate the number of fractures per unit volume, $n(r)$, as a function of size for a fracture set the probability density function must be multiplied by n_0, the average number of fractures per unit volume of rock:

$$n(r) = n_0 \frac{k\, r_0^k}{r^{k+1}} \tag{2}$$

The factor n_0 is obtained from the fracture intensity, P_{32}, i.e. the total fracture area per unit volume of rock, through:

$$P_{32} = \int_{r_0}^{r_{upper}} n_0 \frac{k\, r_0^k}{r^{k+1}} \pi r^2 dr = \frac{n_0 \pi r_0^k k}{k-2}\left(\frac{1}{r_0^{k-2}} - \frac{1}{r_{upper}^{k-2}}\right) \tag{3}$$

where r_{upper} is the upper limit of fracture sizes included in the empirical determination of the P_{32}-value. In practice, r_{upper} is much larger than r_0, and Equation (3) can be simplified to:

$$P_{32} = n_0 \pi r_0^2 \frac{k}{k-2} \tag{4}$$

The number of fractures per unit volume of rock of radii in the interval $[r, r+dr]$ is thus given by:

$$n(r)dr = P_{32} \frac{(k-2) r_0^{k-2}}{\pi r^{k+1}} dr \tag{5}$$

2.1.2 Critical fracture movements

Canisters are not to be exposed to fracture displacements exceeding a certain critical value d_{Crit}. Results in /Börgesson et al. 2004/ suggest that d_{Crit} is typically 0.1 m. The maximum earthquake related displacement of a fracture of radius r, occurring at the centre of the fracture, is in the literature often expressed by a relationship of the form

$$d_{Max} = b r^c \tag{6}$$

where b and c are constants governed by tectonic setting, type of faulting, material properties, etc. Any fracture or fracture zone large enough to host an earthquake of any significance is assumed to be readily observable and thus avoidable at canister deposition /Munier and Hökmark, 2004/. Secondary movements can however occur in smaller fractures in the vicinity of the primary displacement. If such fractures are not detected and avoided, canister ruptures due to secondary fracture movements could occur in the event of large earthquakes near a repository. In quantitative studies of such movements, it is often assumed that the host rock is a linear elastic medium /Munier and Hökmark, 2004/. This means that, for the secondary movements, $c = 1$ in Equation (6) /Pollard and Segall, 1987/. Furthermore, results in /Munier and Hökmark, 2004/ indicate that, for situations

of relevance here, b can typically be taken to be such that a fracture of radius 100 m has a maximum displacement of 0.1 m if located near an earthquake of magnitude 6 or larger; i.e. b is typically 0.001.

This also means that there is a minimum fracture size, r_{Min}, that has to be avoided such that

$$r_{Min} = \frac{d_{Crit}}{b} \tag{7}$$

For a linear elastic medium, the displacement along a fracture of radius r varies from d_{Max} at the fracture centre ($r' = 0$) to zero at its periphery ($r' = r$) according to /Itasca, 2004/

$$\frac{d(r')}{d_{Max}} = \sqrt{1 - \left(\frac{r'}{r}\right)^2} \tag{8}$$

This means that d_{Crit} occurs at r'_{Crit} given by

$$r'_{Crit} = r\sqrt{1 - \left(\frac{d_{Crit}}{d_{Max}}\right)^2} = r\sqrt{1 - \left(\frac{r_{Min}}{r}\right)^2} = \sqrt{r^2 - r_{Min}^2} \qquad r > r_{Min} \tag{9}$$

2.1.3 Total critical fracture area

The total critical fracture area per unit volume of rock, a, is now obtained as

$$a = \int_{r_{Min}}^{r_{Max}} n(r)\,\pi\left(r'_{Crit}\right)^2 dr = \int_{r_{Min}}^{r_{Max}} n(r)\,\pi\left(r^2 - r_{Min}^2\right) dr \tag{10}$$

Here, r_{Max} is a maximum size above which a fracture is assumed to be readily observable. Inserting $n(r)$ from Equation (5) into Equation (10) and evaluating yields

$$a = P_{32}(k-2)\left\{\left(\frac{r_0}{r_{Max}}\right)^{k-2}\left[\frac{1}{2-k} + \left(\frac{r_{Min}}{r_{Max}}\right)^2 \frac{1}{k}\right] - \left(\frac{r_0}{r_{Min}}\right)^{k-2}\left[\frac{1}{2-k} + \frac{1}{k}\right]\right\} \tag{11}$$

It is noted that a depends sensitively on k, see further section 3.

2.1.4 Log-normally distributed fracture sizes

In analogy with the case of power-law distributed fracture sizes, an expression for a is derived for a log-normal fracture size distribution in Appendix A.

2.2 Width of canister intersection zone

2.2.1 Fisher distributed fracture orientations

Each fracture set is characterised by a principal orientation around which the orientations of the fractures within the set are concentrated. The normal vector of a fracture with the principal orientation is described by a plunge angle, θ_p, describing the inclination of the normal vector with respect to the horizontal plane, and a trend angle describing its direction in the horizontal plane. In the following, only the plunge angle is of interest.

The concentration of fractures in a set around the principal orientation can be described by a so called Fisher distribution /Fisher et al. 1987/, for which the probability density function, $g(\theta')$ is

$$g(\theta') = \frac{\kappa \sin\theta' \exp(\kappa \cos\theta')}{\exp(\kappa) - \exp(-\kappa)} \quad (12)$$

where θ' is the angle between the fracture normal and the normal of the principal orientation and κ is a measure of the degree of concentration around the principal orientation. Figure 2-1 shows the Fisher distribution for a number of κ-values.

A κ-value of zero corresponds to a uniform distribution on the unit sphere and a κ-value approaching infinity corresponds to a situation where all fractures in a set have the principal orientation. For a given value of θ', the distribution of the azimuthal angle, φ' is assumed uniform.

The likelihood of finding a fracture with a normal of an orientation described by the intervals $[\theta' + d\theta']$ and $[\varphi' + d\varphi']$ is thus

$$dp(\theta', \varphi') = g(\theta') d\theta' \frac{1}{2\pi} d\varphi' \quad (13)$$

2.2.2 Canister intersection zones

A fracture larger than the prescribed size limit must not intersect a deposition hole, or, more correctly, its extension in the deposition hole must not intersect the cylindrical canister. To avoid intersection of a *perfectly horizontal* fracture with deposited canisters, canister midpoints may not be located closer to the fracture than half the canister height, $h_{Can}/2$, on either side of the fracture. The width of the canister intersection zone, L, is thus for this fracture equal to h_{Can}.

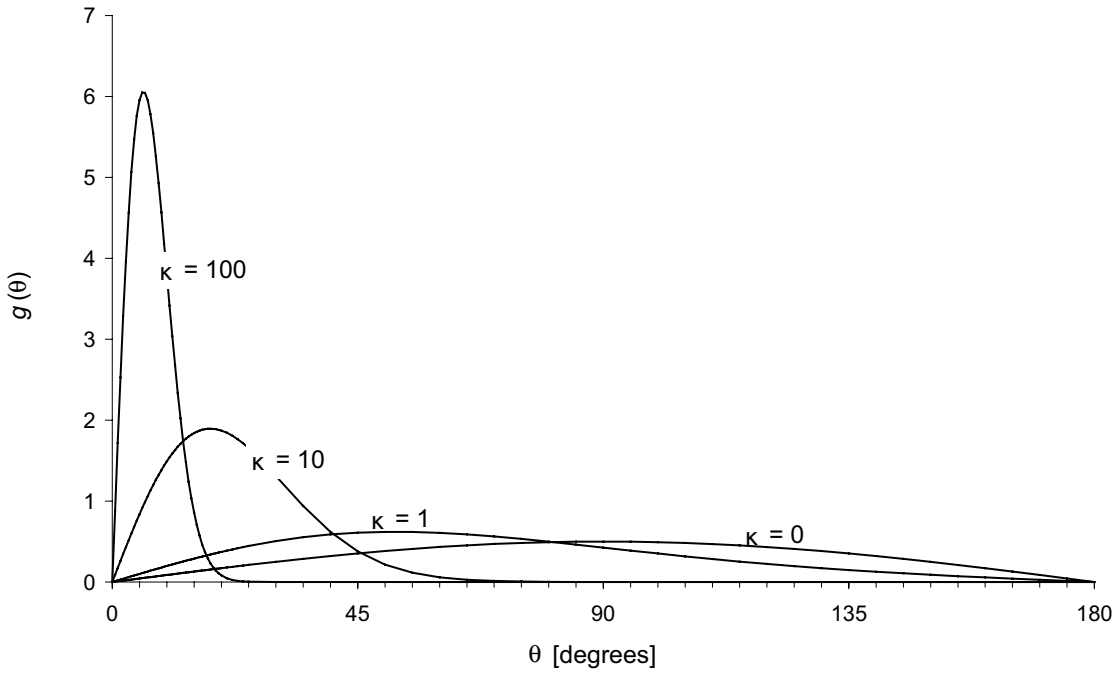

Figure 2-1. *The Fisher distribution for a number of values of the parameter κ.*

For a *perfectly vertical* fracture, the corresponding width is similarly equal to the canister diameter, d_{Can}.

Generally, a planar fracture for which the normal vector is inclined an angle θ with respect to the horizontal plane has an intersection zone width $L(\theta)$, see Figure 2-2,

$$L(\theta) = h_{Can}\left|\sin\theta\right| + d_{Can}\left|\cos\theta\right| = h_{Can}\left|\sin\theta\right| + d_{Can}\sqrt{1-\sin^2\theta} \qquad (14)$$

Figure 2-3 shows $L(\theta)$ for the KBS-3 canister dimensions d_{Can} = 1.05 m and h_{Can} = 4.833 m. Note that the first maximum occurs at $\theta_p = \arctan(h_{Can} / d_{Can}) \approx 78°$, i.e. when the fracture normal is parallel to a canister diagonal. This maximum is equal to $\sqrt{d_{Can}^2 + h_{Can}^2} \approx 4.95$ m. The minima at 0°, 180° and 360° (vertical fractures) are equal to d_{Can} and the local minima at 90° and 270° (horizontal fractures) are equal to h_{Can}.

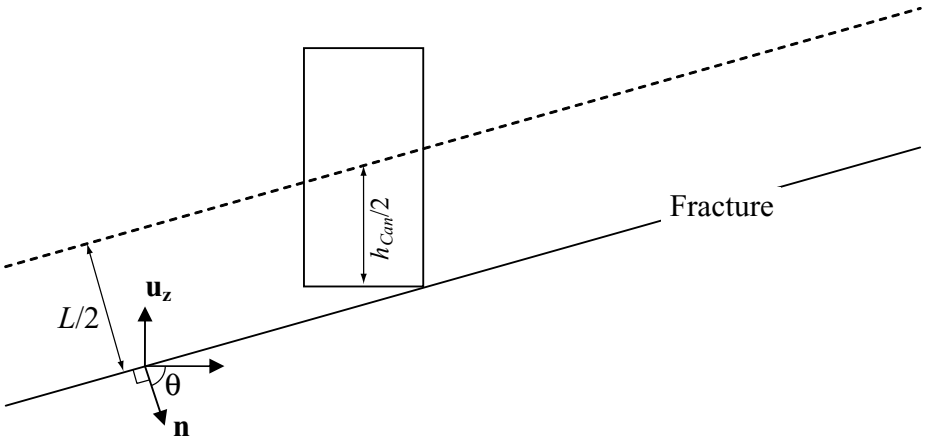

Figure 2-2. *The intersection zone width, L, for a fracture for which the normal is inclined an angle θ with respect to the horizontal plane. Canisters should not be intersected by the fracture, meaning that their midpoints should not be closer than L / 2 to the fracture.*

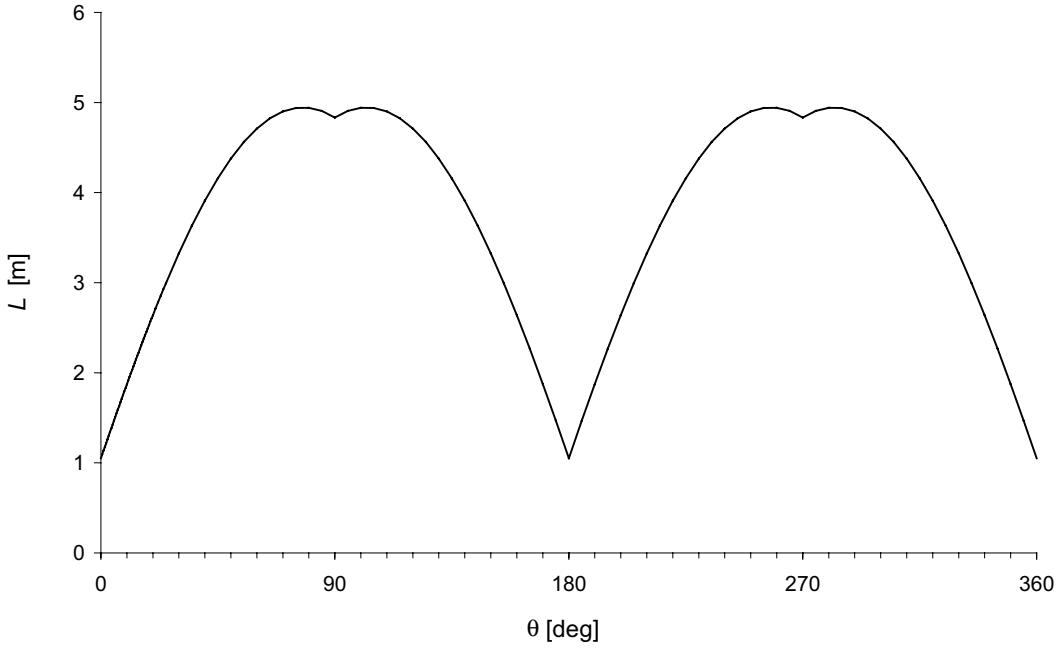

Figure 2-3. *The intersection zone width, L, as a function of the orientation of the fracture normal with respect to the horizontal plane, θ.*

2.2.3 Mean width of canister intersection zone

In order to calculate the average intersection zone width over a fracture set, $<L>$, $L(\theta)$ must be averaged over the angular distribution expressed by Equation (13).

$$< L >= \int_{\theta'=0}^{\pi} \int_{\varphi'=0}^{2\pi} \left(h_{Can} |\sin\theta| + d_{Can} \sqrt{1-\sin^2\theta} \right) \frac{\kappa \sin\theta' \exp(\kappa \cos\theta')}{\exp(\kappa) - \exp(-\kappa)} \frac{1}{2\pi} d\varphi' d\theta' \quad (15)$$

Consider a Cartesian coordinate system with the *z'* direction coinciding with the normal of the principal orientation, *y'* in the horizontal plane and *x'* with a negative projection in the vertical direction. In this system, the vertical unit vector is

$$\mathbf{u_z} = \left(-\cos\theta_p, 0, -\sin\theta_p \right) \quad (16)$$

where θ_p is the angle between the normal of the principal orientation and the horizontal plane. A fracture for which the orientation of the normal vector, **n**, is described by the polar and azimuthal angles θ' and φ' with respect to the principal orientation has the coordinates

$$\mathbf{n} = \left(\sin\theta'\cos\varphi', \sin\theta'\sin\varphi', \cos\theta' \right) \quad (17)$$

The vertical projection of the unit vector **n**, i.e. $\cos(90° - \theta) = \sin\theta$ is obtained as the scalar product of the two unit vectors **n** and $\mathbf{u_z}$:

$$\sin\theta = \mathbf{u_z} \cdot \mathbf{n} = -\cos\theta_p \sin\theta'\cos\varphi' - \sin\theta_p \cos\theta' \quad (18)$$

Inserting Equation (18) into Equation (15) yields a double integral that generally must be solved numerically.

The special case of $\theta_p = \pi/2$ and $d_{Can} = 0$ can, however, be solved analytically:

$$< L >= \int_{\theta'=0}^{\pi} \int_{\varphi'=0}^{2\pi} h_{Can} |\sin\theta| \frac{\kappa \sin\theta' \exp(\kappa \cos\theta')}{\exp(\kappa) - \exp(-\kappa)} \frac{1}{2\pi} d\varphi' d\theta'$$

$$= \int_0^{\pi/2} h_{Can} \cos\theta' \frac{\kappa \sin\theta' \exp(\kappa \cos\theta')}{\exp(\kappa) - \exp(-\kappa)} d\theta' - \int_{\pi/2}^{\pi} h_{Can} \cos\theta' \frac{\kappa \sin\theta' \exp(\kappa \cos\theta')}{\exp(\kappa) - \exp(-\kappa)} d\theta'$$

$$= h_{Can} \left[\frac{(1 - \kappa\cos\theta')\exp(\kappa\cos\theta')}{\kappa(\exp(\kappa) - \exp(-\kappa))} \right]_0^{\pi/2} - h_{Can} \left[\frac{(1 - \kappa\cos\theta')\exp(\kappa\cos\theta')}{\kappa(\exp(\kappa) - \exp(-\kappa))} \right]_{\pi/2}^{\pi}$$

$$= h_{Can} \left(1 + \frac{1}{\kappa \sinh\kappa} - \frac{1}{\kappa \tanh\kappa} \right) \quad (19)$$

This special case can be used to check the results of the numerical integration, and it is also interesting since it provides an approximate solution for horizontal fractures. The total fraction of rock volume covered by intersection zones is often dominated by a set of fractures that is nearly horizontal.

The double integral in Equation (15) was solved numerically in 100 × 100 points using the trapezoid rule.[1] Applying the routine to the analytically solvable case in Equation (19) yielded relative errors smaller than 10^{-3}.

[1] For κ-values > 10, the θ-value for which $\kappa \frac{\exp(\kappa\cos\theta)}{\exp(\kappa) - \exp(-\kappa)} = 10^{-4}$ was determined and the integration w.r.t. θ was truncated at this θ-value, making a more efficient use of the 100 points of integration w.r.t. θ. The absolute error on $<L>$ introduced with this truncation is bounded by $10^{-4}\pi\sqrt{d_{Can}^2 + h_{Can}^2} \approx 1.6 \cdot 10^{-3}$ since the integrand is lower than $10^{-4}\sqrt{d_{Can}^2 + h_{Can}^2}$ for θ exceeding the truncation limit and the integration interval is $0 < \theta < \pi$.

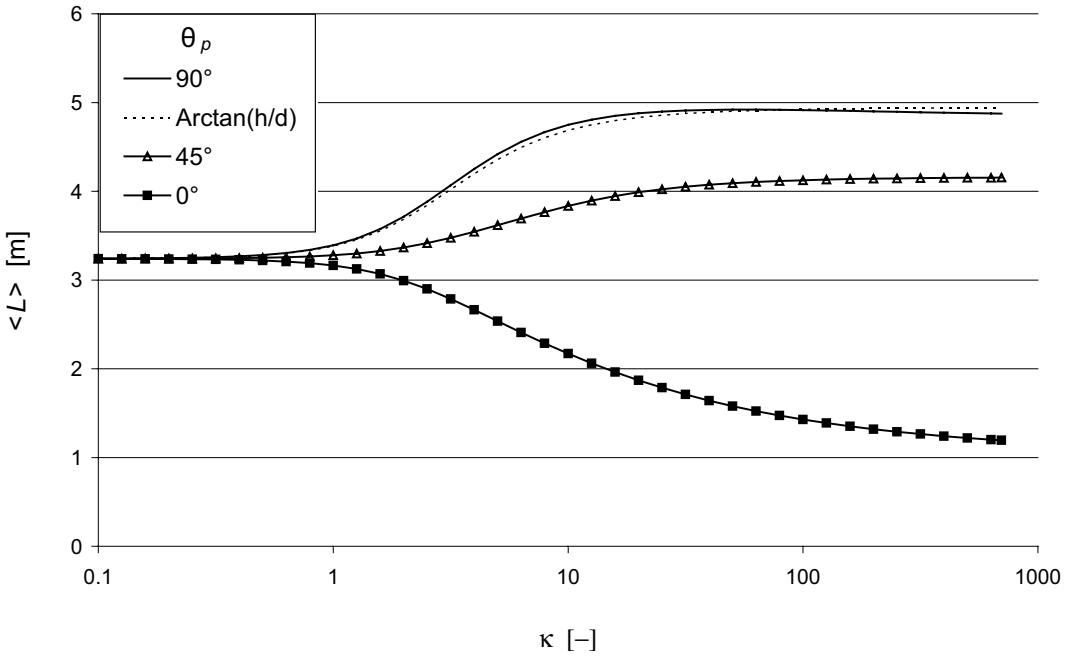

Figure 2-4. *The average intersection zone width, <L>, as a function of the concentration factor κ for a number of fracture set principal orientations.*

Figure 2-4 demonstrates how <*L*> depends on κ for the KBS-3 canister dimensions d_{Can} = 1.05 m and h_{Can} = 4.833 m for a number of plunge angles θ_p. Note the small difference between a horizontal set (θ_p = 90°) and a set with a plunge angle equal to the most unfavourable orientation (θ_p = arctan(h_{Can} / d_{Can}) ≈ 78°).

2.3 Fraction of rock volume within intersection zones

The expectation value of the fraction of the host rock volume where canister intersection would occur, ε, can now be calculated by multiplying the specific area a from Equation (11) by <*L*> from Equation (15):

$$\varepsilon = a \langle L \rangle \tag{20}$$

The quantity ε can be interpreted in the following way: If a repository is located in a host rock without consideration of fractures intersecting deposition holes, then ε represents the expectation value of the portion of canister positions that are intersected by discriminating fractures.

An evaluation of ε for preliminary data from one of SKB's candidate sites for a deep repository (rock domain 29 at the Forsmark site) is shown in Table 2-1. The calculated volume fraction of rock covered by canister intersection zones is 1.91 percent in this example. If 4,500 canisters are deposited without considering intersecting fractures, this ε-value corresponds to roughly 86 canisters.

To elucidate the importance of details of the angular distribution, also the avoidance fractions assuming that *i)* all fractures in a set have the principal orientation, ε_P, with an intersection zone width L_P obtained by inserting θ_p in Equation (14) and *ii)* all fractures are approximated as either horizontal or vertical, $\varepsilon_\perp$, were calculated. As seen in the table, these approximations yield results comparable to the correctly determined ε-value for this example.

Figure 2-5 shows how the different fracture sets and fracture sizes contribute to the total ε in the calculation example.

Table 2-1. Calculation of ε in for a preliminary DFN model from the Forsmark site. Additional input data are given in Table 2-2.

		Fracture sets Total	NS	NE	NW	EW	SubH
r_0	m		0.318	0.318	0.318	0.318	0.318
k	–		2.88	3.02	2.81	2.95	2.92
$P_{32,all}$	m^{-1}	3.95	0.602	2.07	0.448	0.226	0.605
a	m^2/m^3		0.00174	0.00277	0.00189	0.000445	0.00140
θ_P	°		1.7	2.7	2.2	0.7	90
Trend	°		87.2	135.2	40.6	190.4	342.9
κ	–		21.66	21.54	23.9	30.63	8.18
$<L>$	m		1.85	1.86	1.82	1.72	4.68
L_P	m		1.19	1.28	1.23	1.11	4.83
ε	–	**0.0191**	0.00321	0.00514	0.00342	0.00077	0.00657
ε_P	–	**0.0152**	0.00207	0.00353	0.00233	0.00049	0.00679
$\varepsilon_\perp$	–	**0.0140**	0.00182	0.00290	0.00198	0.00047	0.00679

Table 2-2. Additional input data for the calculation presented in Table 2-1.

Maximum fracture radius, r_{Max}	500 m
Minimum fracture radius, r_{Min}	100 m
Canister diameter, d_{Can}	1.05 m
Canister height, h_{Can}	4.833 m
Constant in fracture radius/displacement relationship, b	0.001
Critical shear distance at deposition hole, d_{Crit}	0.1 m

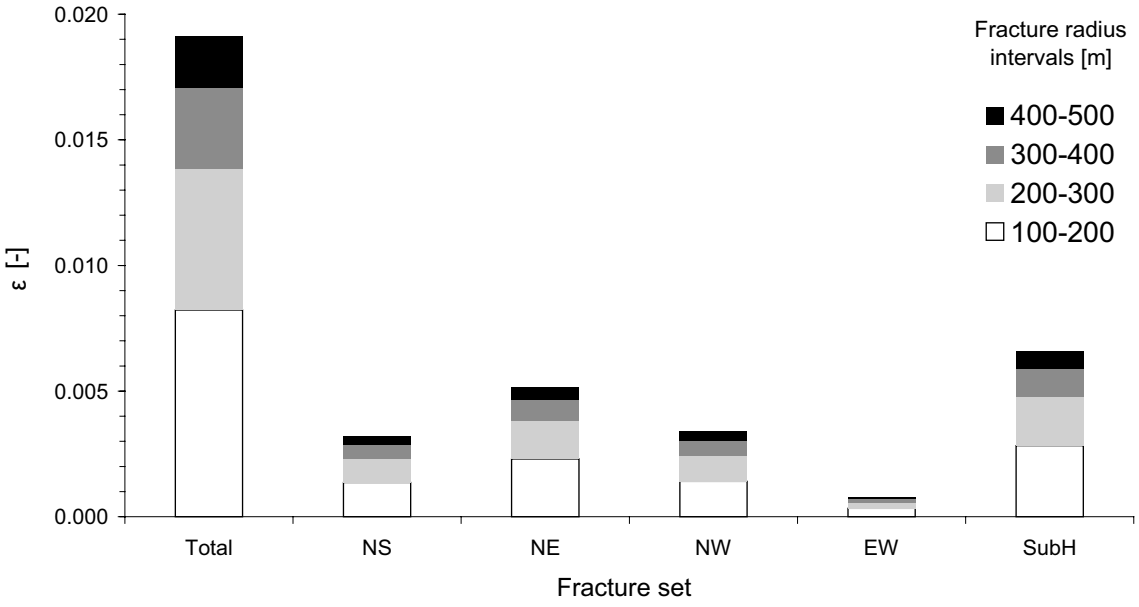

Figure 2-5. *Partitioning of total ε into fracture sets and fracture radius intervals.*

3 Sensitivity analyses

Using the case presented in Table 2-1 and Table 2-2 as a basis, the sensitivity of the resulting ε-values to several of the input parameters has been analysed. The results presented below can be used as a basis for feedback to further planning of the fracture sampling and modelling activities that lead to the formulation of the discrete fracture network models used as input to the calculation of ε and other important factors for the long-term safety of a KBS-3 repository. The meaning and physical reasonableness of the selected input parameter spans are, however, not discussed in detail here.

3.1 Sensitivity to the maximum fracture radius, r_{Max}

The sensitivity of ε to the maximum fracture radius in the model, r_{Max}, is shown in Figure 3-1. The maximum radius has been varied around the base case value, i.e. r_{Max} = 500 m. Note that this figure contains essentially the same information as Figure 2-5.

3.2 Sensitivity to the exponent in the fracture size model, k

The sensitivity of ε to the exponent in the fracture size model, k, is shown in Figure 3-2. The exponent has been varied ±20 percent around the base case value for each fracture set. The base case k-values are around 3, see Table 2-1. Note the high sensitivity of the results to changes in k.

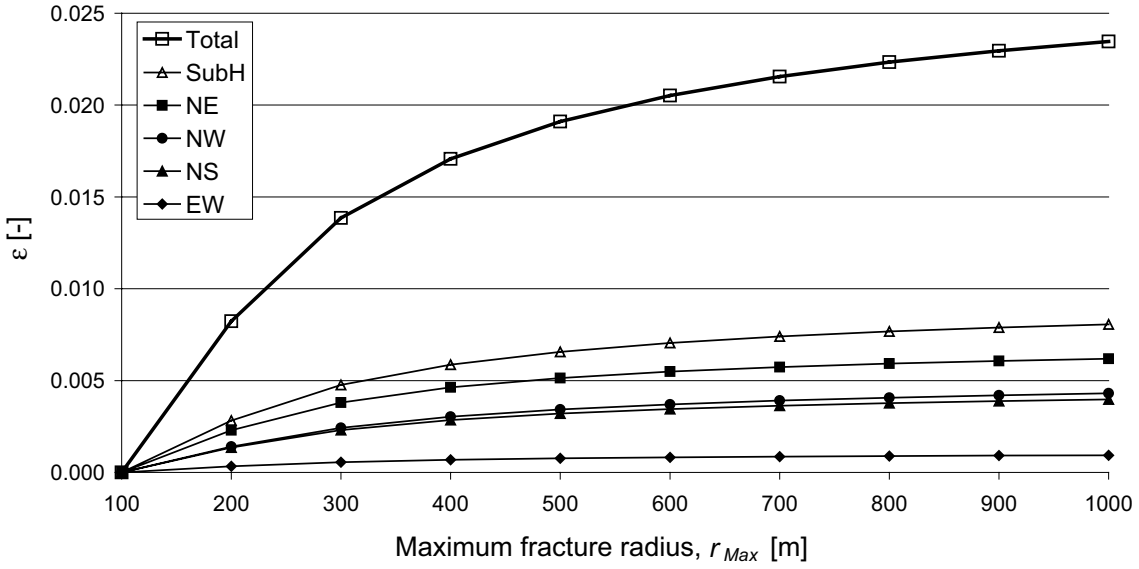

Figure 3-1. *The sensitivity of ε to the maximum fracture radius in the model, r_{Max}. An r_{Max}-value of 500 m is used in the base case.*

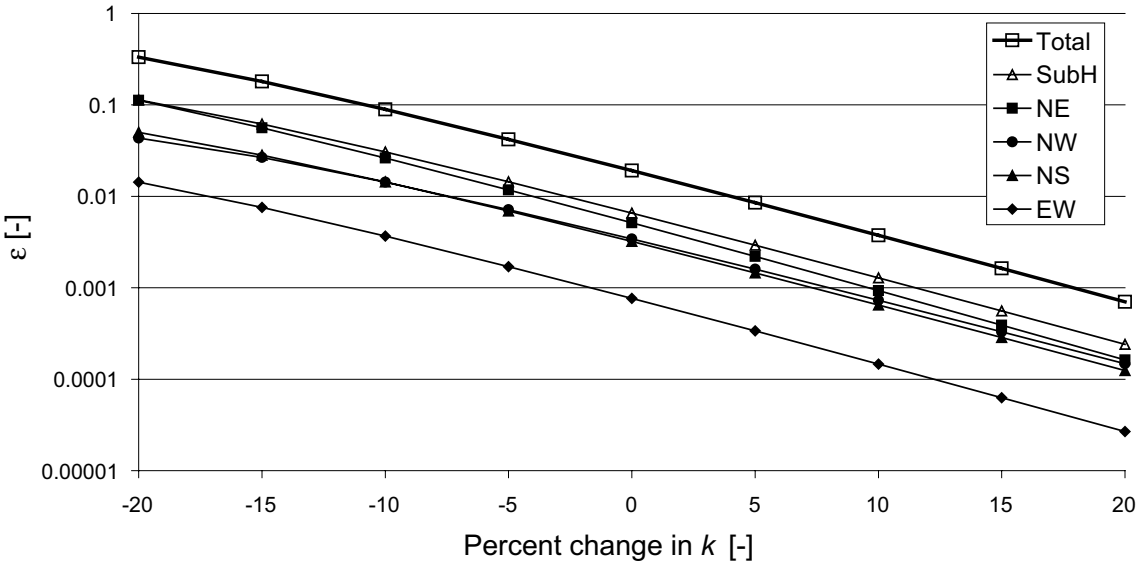

Figure 3-2. *The sensitivity of ε to the exponent in the fracture size model, k. The base case k values are around 3 and vary slightly between fracture sets.*

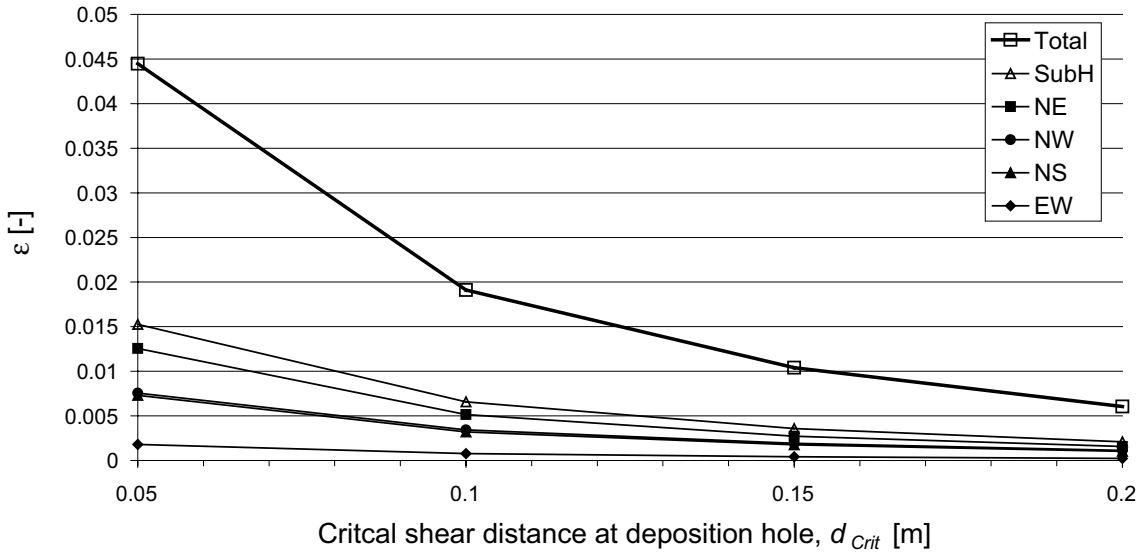

Figure 3-3. *The sensitivity of ε to the critical shear distance at the deposition hole, d_{Crit}. A d_{Crit} -value of 0.1 m is used in the base case.*

3.3 Sensitivity to the critical shear distance at the deposition hole, d_{Crit}

The sensitivity of ε to the critical shear distance at the deposition hole, d_{Crit}, and thus to r_{Min} through Equation (7), is shown in Figure 3-3. The critical distance has been varied around the base case value, i.e. d_{Crit} = 0.1 m. This value was cautiously selected from results of modellings of the response of the buffer/canister system to shear movements around depositions holes /Börgesson et al. 2004/. Many of the modelling cases indicated that the canister would sustain d_{Crit}-values of 0.2 m.

3.4 Sensitivity to the constant in the fracture radius/ displacement relationship, *b*

The sensitivity of ε to the constant in the fracture radius/displacement relationship, b, is shown in Figure 3-4. The b-value was varied around the base case value, i.e. $b = 0.001$.

3.5 Sensitivity to parameters of the distribution of fracture orientations

The sensitivity of $<L>$ to the κ-value is shown in Figure 2-4, section 2.2.2, for a number of values of the plunge angle, θ_p. As seen in Figure 2-4, these dependences are rather weak for typical κ-values, e.g. those in Table 2-1 and for all plunge angles in the figure. The results are thus not very sensitive to details of the angular distributions. This means that an angular distribution that is close to a Fisher distribution can be approximated with the latter, at least when the fracture model is to be used for calculations of ε.

It is further noted that the trend angle does not enter the analytic model. ε is thus independent of the trend angle. Another way of expressing this is to say that ε is independent of repository layout as long as the cylindrical canisters are oriented vertically. This is maybe most readily realised when a single canister is considered; since it is rotationally symmetric around the vertical axis, the likelihood of it being intersected by a fracture is independent of the trend angle that merely represents a rotation around the vertical axis. This is verified by simulation results presented in chapter 4.

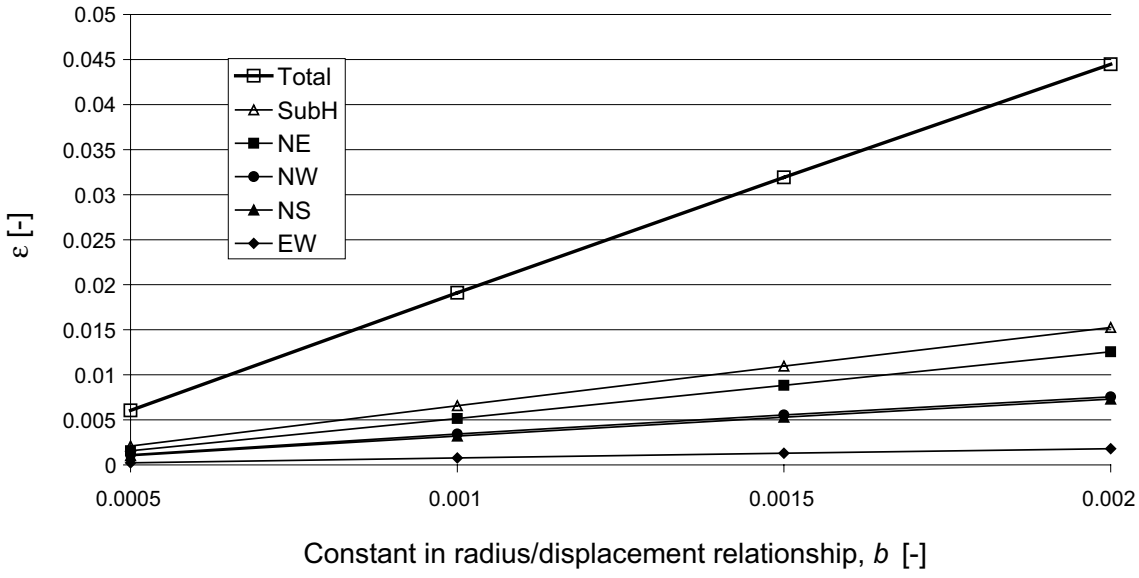

Figure 3-4. *The sensitivity of ε to the constant in the fracture radius/displacement relationship, b. A b-value of 0.001 is used in the base case.*

4 Simulations

The theory presented above yields the mean fraction of canisters in deposition holes intersected by fractures that could potentially host detrimental shear movements if triggered by a nearby earthquake.

Through simulations, it is possible to determine the entire statistical distribution of the number of intersected canisters for an ensemble of realisations of the host rock with fracture statistics according to the preceding sections.

A simulation will also yield a value of the mean fraction of canisters. That value can be compared to the one calculated analytically, thereby providing a way of benchmarking these two methods against each other.

Potentially detrimental fractures will, to the extent possible, be avoided when determining canister positions. The likelihood of detecting discriminating fractures depends largely on the way in which they intersect the entire repository configuration. In particular, it is interesting to investigate the number of deposition holes a particular discriminating fracture could intersect. Also this information is accessible statistically through simulations.

The theory behind the simulations is explained in Appendix B. The treatment concerns power-law distributed fracture sizes and Fisher distributed fracture orientations, but can readily be modified to apply to other distribution types.

4.1 Simulation procedure and results

A repository layout with canisters separated by 6 m along one horizontal direction and by 40 m in the perpendicular direction was used in the simulations.

Several rotations of this structure in the xy-plane were simulated with a rotation of 0° corresponding to the 6 m separation being along the x-axis.

50,000 fractures were generated of each set in Table 2-1 and the number of intersected canisters was determined for each fracture.

The simulation yielded ε-values in agreement to around one percent with those calculated analytically with Equation (20), see Figure 4-1. The result also demonstrates that ε is, as expected, independent of repository layout.

The quantity ε represents the expectation value of the portion of canisters intersected by discriminating fractures. The entire distribution of this quantity is also of interest. The actual number of intersected canisters was therefore simulated for 50,000 realisations of a host rock with fracture statistics according to Table 2-1. The simulation was carried out in two steps.

In the first step, 50,000 fracture samples from each fracture set were generated within a volume sufficiently large to house all discriminating fractures for the above repository layout, using the enhanced sampling technique described in Appendix B. For each fracture, the number of canister intersections was recorded.

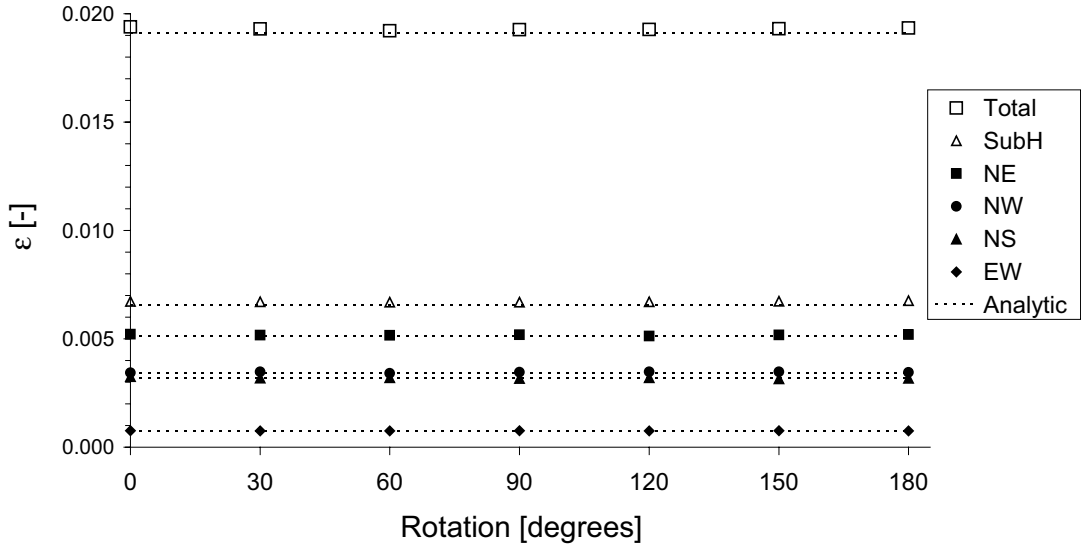

Figure 4-1. *Simulations of ε for 4,500 canisters and for seven repository orientations.*

In the second step, the expectation value of the number of fractures from each set within the repository volume was determined using Equation (B-30) in Appendix B. In a particular realisation of the host rock, the actual number of fractures from this set was drawn from a Poisson distribution with a mean value equal to this expectation value. The so determined number of fractures with associated numbers of intersected canisters was then sampled from the set-specific populations generated in the first step. Summing the number of intersected canisters over all sets and over all sampled fractures within each set yields a total number of intersected canisters, *N*, for a particular realisation of the host rock. This was repeated for 50,000 realisations, yielding the distribution shown in Figure 4-2.

The mean value of *N* for the total distribution in Figure 4-2 is 85.3 canisters, corresponding to an ε-value of 85.3/4,500 ≈ 0.0190, in good agreement with the analytically calculated value of 0.0191 given in Table 2-1. The distribution of *N* is, to a good approximation, a log-normal distribution, as shown by the fitted log-normal distribution in Figure 4-2.

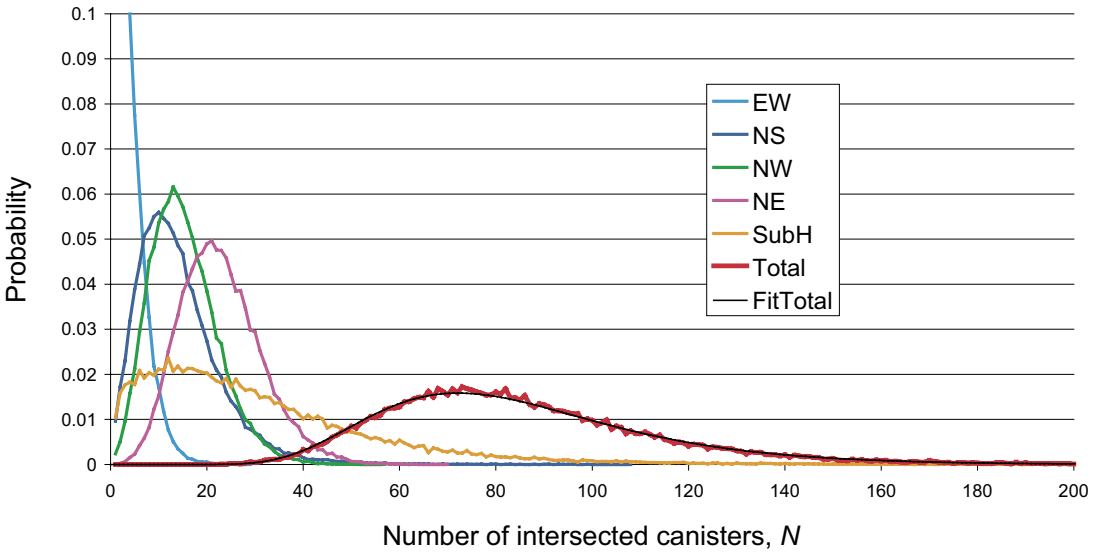

Figure 4-2. *Distributions of number of canisters intersected by discriminating fractures, without considering the likelihood of detecting and avoiding such fractures at deposition. The thin, black line "FitTotal" shows a log-normal distribution fitted to the "Total" distribution.*

5 Discussion and conclusions

This report has demonstrated that the likelihood of canisters intersecting host rock fractures of a specified size in a KBS-3 type repository is calculable analytically for the frequently used descriptions of fracture statistics treated here.

Sensitivity analyses point to important model parameters to determine for these distribution types. In general, the results are more sensitive to uncertainties in parameters relating to the fracture size distributions than to those relating to the orientation distributions.

Furthermore, it has been demonstrated that the entire probability distribution of the number of intersected canisters is accessible through simulations. These simulations confirm the analytically derived results of mean values.

From field investigations, observations of fracture sizes are often available in the interval tens of centimetres to tens of metres and of structures larger than several hundred meters. It is however fractures with radii between these two sets, i.e. in the interval tens up to a few hundred metres that are critical for avoiding detrimental earthquake induced rock shear movements. For safety assessments of a KBS-3 repository, it is thus essential to gain confidence in the description of fracture statistics in this size interval.

It is furthermore essential to develop methods for avoiding discriminating fractures when depositing canisters, based on observable indications of such fractures in and around deposition holes. With descriptions of such methods and their reliability, the calculation presented here could readily be developed to include the likelihood of detecting and avoiding discriminating fractures, a likelihood that should increase with fracture size.

There are several uncertainties in the overall treatment of earthquake induced fracture movements that are not addressed in this report. These include the likelihood of occurrence of such events in the vicinity of a repository, which in particular needs to be considered in a post glacial climate phase. Furthermore, all fractures are assumed to reactivate as if their location and angular orientation relative to the primary earthquake were unfavourable. All fractures distant from the earthquake generating fault are pessimistically assumed to slip by the same amount, determined only by the secondary fracture size. The assumption that the rock responds as a linear-elastic medium, with implications on *i)* the relationship between fracture size and maximum displacement and *ii)* on the displacement as a function of location along the fracture, is also uncertain.

6 QA aspects

The analytic calculation methods presented in chapter 2 and the simulations presented in chapter 4 are largely independent, yet they produce practically identical expectation values. The analytic method is based on evaluations of a, Equation (11), and $\langle L \rangle$, Equation (15), whereas the simulations do not use these concepts. The analytic model does not apply any of the simulation theory, including the test for canister intersections, described in Appendix B. The fact that these two largely independent methods yield practically identical expectation values is therefore an important contribution to the overall quality assurance and confidence in the methods and codes presented in this report.

Commercially available software has been used for both the analytic calculations (Microsoft Excel) and the simulations (@Risk simulation engine used as plug-in to Microsoft Excel). Both these tools are widely tested and have large user groups.

The calculation of $\langle L \rangle$, involving a numerical evaluation of a double integral, has been tested against the analytic solution for the special case described by Equation (19) and evaluated for limits of low and high κ-values. The double integral used to determine $\langle L \rangle$ has also been verified by an independently set-up calculation with an alternative tool (Matlab).

7 References

Börgesson L, Johannesson L-E, Hernelind J, 2004. "Earthquake induced rock shear through a deposition hole. Effect on the canister and the buffer", SKB TR-04-02, Svensk Kärnbränslehantering AB.

Fisher N I, Lewis T, Embleton B J, 1987. Statistical Analysis of Spherical Data. Cambridge University Press, p 329.

Itasca, 2004. UDEC, Universal Distinct Element Code. Version 3.1 users manual. Itasca consulting Group Inc, Minneapolis.

Munier R, Hökmark H, 2004. Respect distances. Rationale and means of computation. SKB R-04-17, Svensk Kärnbränslehantering AB.

Pollard D D, Segall P, 1987. Theoretical displacements near fractures in rock: with applications to faults joints, veins, dikes and solution surfaces. Fracture Mechanics of Rock. Academic Press Inc. Ltd, London.

SKB, 2004. Interim Main Report of the Safety Assessment SR-Can. SKB TR-04-11, Svensk Kärnbränslehantering AB.

Appendix A

Derivation of *a* for a log-normal size distribution

In analogy with the case of power-law distributed fracture sizes, an expression for a is derived for a log-normal fracture size distribution in this Appendix.

Consider a log-normal size distribution, $f_{LN}(r)$:

$$f_{LN}(r) = \frac{1}{r\sqrt{2\pi}\sigma'} \exp\left[-\frac{1}{2}\left(\frac{\ln(r) - \mu'}{\sigma'} \right)^2 \right] \tag{A-1}$$

with

$$\mu' = \ln\left(\frac{\mu^2}{\sqrt{\mu^2 + \sigma^2}} \right) \tag{A-2}$$

and

$$\sigma' = \frac{1}{2}\ln\left(1 + \frac{\sigma^2}{\mu^2} \right) \tag{A-3}$$

where μ and σ are the mean value and the standard deviation of the size distribution in arithmetic space.

In analogy with the treatment of power-law distributed fracture sizes above, an average fracture density, n_0, is determined for the log-normal distribution through

$$n_0 = \frac{P_{32}}{\int_0^\infty \pi r^2 f_{LN}(r) dr} \tag{A-4}$$

As for the power-law distributed fracture sizes, a is determined by

$$a = \int_{r_{Min}}^{r_{Max}} n(r)\pi\left(r'_{Crit}\right)^2 dr = \int_{r_{Min}}^{r_{Max}} n(r)\pi\left(r^2 - r_{Min}^2\right) dr = P_{32} \frac{\int_{r_{Min}}^{r_{Max}} \pi\left(r^2 - r_{Min}^2\right) f_{LN}(r) dr}{\int_0^\infty \pi r^2 f_{LN}(r) dr}$$

$$= P_{32} \frac{\int_{r_{Min}}^{r_{Max}} r^2 f_{LN}(r) dr - r_{Min}^2 \int_{r_{Min}}^{r_{Max}} f_{LN}(r) dr}{\int_0^\infty r^2 f_{LN}(r) dr} \tag{A-5}$$

These integrals may be expressed in terms of the error function according to the following:

Let

$$f_{qLN}(r) = r^q f_{LN}(r) = \frac{r^q}{r\sqrt{2\pi}\sigma'} \exp\left[-\frac{1}{2}\left(\frac{\ln(r) - \mu'}{\sigma'} \right)^2 \right] \tag{A-6}$$

Then

$$\int_0^r f_{qLN}(\tau) d\tau = \int_0^r \frac{\tau^q}{\tau\sqrt{2\pi}\sigma'} \exp\left[-\frac{1}{2}\left(\frac{\ln(\tau) - \mu'}{\sigma'} \right)^2 \right] d\tau \tag{A-7}$$

With the substitution

$$t = \frac{\ln(\tau) - \mu'}{\sigma'}; \quad \tau = \exp(\sigma' t + \mu'); \quad d\tau = \sigma' \exp(\sigma' t + \mu') dt \tag{A-8}$$

we obtain

$$\int_0^r f_{qLN}(\tau) d\tau = \int_{-\infty}^{\frac{\ln(r)-\mu'}{\sigma'}} \frac{\exp(q\sigma' t + q\mu')}{\sqrt{2\pi}} \exp\left[-\frac{1}{2} t^2 \right] dt = \frac{\exp(q\mu')}{\sqrt{2\pi}} \int_{-\infty}^{\frac{\ln(r)-\mu'}{\sigma'}} \exp\left[-\frac{1}{2} t^2 + q\sigma' t \right] dt$$

$$= \frac{1}{\sqrt{2\pi}} \exp\left(q\mu' + \frac{q^2\sigma'^2}{2} \right) \int_{-\infty}^{\frac{\ln(r)-\mu'}{\sigma'}} \exp\left[-\frac{1}{2}(t - q\sigma')^2 \right] dt$$

$$= \frac{1}{\sqrt{2\pi}} \exp\left(q\mu' + \frac{q^2\sigma'^2}{2} \right) \int_{-\infty}^{\frac{\ln(r)-\mu'}{\sigma'} - q\sigma'} \exp\left(-\frac{t^2}{2} \right) dt \tag{A-9}$$

Observing that

$$\frac{1}{\sqrt{2\pi}} \int_{-\infty}^{x} \exp\left(-\frac{t^2}{2} \right) dt \equiv \frac{\mathrm{erf}(t) + 1}{2} \tag{A-10}$$

where $\mathrm{erf}(\cdot)$ is the error function, we finally obtain

$$\int_0^r f_{qLN}(\tau) d\tau = \frac{1}{2} \exp\left(q\mu' + \frac{q^2\sigma'^2}{2} \right) \left[\mathrm{erf}\left(\frac{\ln(r) - \mu'}{\sigma'} - q\sigma' \right) + 1 \right] \tag{A-11}$$

Applying this result to the above integrals we obtain

$$\int_0^\infty r^2 f_{LN}(r) dr = \exp(2\mu' + 2\sigma'^2) \tag{A-12}$$

$$\int_{r_{Min}}^{r_{Max}} r^2 f_{LN}(r)dr = \frac{1}{2}\exp\left(2\mu'+2\sigma'^2\right)\left[\operatorname{erf}\left(\frac{\ln(r_{Max})-\mu'}{\sigma'}-2\sigma'\right)\right.$$

$$\left.-\operatorname{erf}\left(\frac{\ln(r_{Min})-\mu'}{\sigma'}-2\sigma'\right)\right] \qquad \text{(A-13)}$$

and

$$\int_{r_{Min}}^{r_{Max}} f_{LN}(r)dr = \frac{1}{2}\left[\operatorname{erf}\left(\frac{\ln(r_{Max})-\mu'}{\sigma'}\right)-\operatorname{erf}\left(\frac{\ln(r_{Min})-\mu'}{\sigma'}\right)\right] \qquad \text{(A-14)}$$

Inserting Equations (A-12) – (A-14) into Equation (A-5) yields the final expression for *a* in case of a log-normal fracture size distribution.

Appendix B

Simulation theory

A set of fractures with size and directional distributions according to Equations (1) and (13) can be generated by, for each circular fracture, generating a centre point, a radius and a direction of its normal.

Fracture centre points

According to the above sections, fractures with sizes in the interval $r_{Min} < r < r_{Max}$ need to be considered. In a repository where canisters are assumed to be located in a volume bounded by $x = [x_{Min}, x_{Max}]$, $y = [y_{Min}, y_{Max}]$ and $z = [z_{Min}, z_{Max}]$, a representative distribution of fractures in a volume bounded by $x = [x_{Min} - r_{Max}, x_{Max} + r_{Max}]$, etc needs to be generated. This volume would contain the centre points of all fractures that could intersect deposition holes in a fashion that could jeopardise canister integrity.

Assuming a Poissonian spatial structure, i.e. uncorrelated fracture locations, fracture centre points (x_0, y_0, z_0) are generated by sampling from uniform distributions within these intervals, i.e. $x_0 = \text{Uniform}\ (x_{Min} - r_{Max}, x_{Max} + r_{Max})$ etc.

The volume, V, considered in the simulation is thus

$$V = \left(x_{Max} - x_{Min} + 2r_{Max}\right)\left(y_{Max} - y_{Min} + 2r_{Max}\right)\left(z_{Max} - z_{Min} + 2r_{Max}\right) \qquad \text{(B-1)}$$

Fracture sizes

Fractures in the size interval $r = [r_{Min}, r_{Max}]$ can be generated using Equation (1), re-normalised so that only fractures in the sought interval are generated. This is achieved by requiring that the distribution function, $F(r)$, equals 0 for $r = r_{Min}$ and 1 for $r = r_{Max}$:

$$F(r) = \int f(r) = \frac{A}{r^k} + B \qquad \text{(B-2)}$$

yielding

$$F(r) = \frac{\left(\frac{r_{Min}}{r}\right)^k - 1}{\left(\frac{r_{Min}}{r_{Max}}\right)^k - 1} \qquad \text{(B-3)}$$

Solving for r yields

$$r = \frac{r_{Min}}{\left[F(r)\left(\left(\frac{r_{Min}}{r_{Max}}\right)^k - 1\right) + 1\right]^{1/k}} \qquad \text{(B-4)}$$

The required distribution of fracture sizes is thus generated by sampling $F(r)$ from a uniform distribution and calculating *r* with the above expression.

Fracture orientations

A fracture set where fracture orientations are characterised by a Fisher distributed polar angle θ' and a uniformly distributed azimuthal angle φ' with respect to a principal orientation (see section 2.2.1) can be generated according to the following. The distribution function of a Fisher distribution, $G(\theta')$, for which $G(0) = 0$ and $G(\pi) = 1$ is

$$G(\theta') = \frac{\exp(\kappa) - \exp(\kappa \cos\theta')}{\exp(\kappa) - \exp(-\kappa)} \tag{B-5}$$

Solving for θ' yields

$$\theta' = \arccos\left[\frac{\ln\left\{\exp(\kappa) - G(\theta')[\exp(\kappa) - \exp(-\kappa)]\right\}}{\kappa}\right] \tag{B-6}$$

The required distribution of polar angles with respect to the principal orientation is thus generated by sampling $G(\theta')$ from a uniform distribution and calculating θ' with the above expression.

The azimuthal angle φ' is sampled from a uniform distribution between 0 and 2π.

Fracture normals

In the primed coordinate system (see section 2.2.3), the normal vector of the so generated fracture is

$$\mathbf{n}' = (\sin\theta'\cos\varphi', \sin\theta'\sin\varphi', \cos\theta') \tag{B-7}$$

The unit vectors along the co-ordinate axes in the unprimed system are in primed co-ordinates

$$\mathbf{u_x} = (-\sin\theta_p \cos\varphi_p, -\sin\varphi_p, \cos\theta_p \cos\varphi_p) \tag{B-8}$$

$$\mathbf{u_y} = (-\sin\theta_p \sin\varphi_p, \cos\varphi_p, \cos\theta_p \sin\varphi_p) \tag{B-9}$$

$$\mathbf{u_z} = (-\cos\theta_p, 0, -\sin\theta_p) \tag{B-10}$$

The projections of the normal vector on the unit vectors in the unprimed system, i.e. the co-ordinates of the normal vector in the unprimed system are thus obtained as

$$n_x = -\sin\theta'\cos\varphi'\sin\theta_p \cos\varphi_p - \sin\theta'\sin\varphi'\sin\varphi_p + \cos\theta'\cos\theta_p \cos\varphi_p \tag{B-11}$$

$$n_y = -\sin\theta'\cos\varphi'\sin\theta_p \sin\varphi_p + \sin\theta'\sin\varphi'\cos\varphi_p + \cos\theta'\cos\theta_p \sin\varphi_p \tag{B-12}$$

$$n_z = -\sin\theta'\cos\varphi'\cos\theta_p - \cos\theta'\sin\theta_p \tag{B-13}$$

It can be verified that $n_x^2 + n_y^2 + n_z^2 = 1$ which is required since **n** is a unit vector.

Canister intersections

In order to determine whether a canister with centre point located at (x_{Can}, y_{Can}, z_{Can}) is intersected by a generated fracture centred at x_0, y_0, z_0 and with normal (n_x, n_y, n_z), the below scheme is followed.

A first requirement is that the fracture radius be sufficiently large for the fracture to intersect the canister, i.e.

$$r > \sqrt{(x_0 - x_{Can})^2 + (y_0 - y_{Can})^2 + (z_0 - z_{Can})^2} \quad \text{(B-14)}$$

This is an approximate formulation of the requirement since it examines whether the fracture is sufficiently large to reach the canister centre point, whereas other parts of the canister may be closer to the fracture. Since the canister dimensions are in general much smaller than the fracture radius, the approximation however only introduces minor errors.

In addition, it is required that the fracture orientation is such that the fracture actually intersects a canister. In order to test this for a specific fracture and a particular canister location, the intersection ellipse between an infinite plane containing the fracture and an infinite cylinder containing the canister lateral surface is determined. The maximum and minimum *z* co-ordinates of the intersection ellipse are determined and a simple test can be applied to these co-ordinates in order to determine whether a canister intersection occurs. Details are provided in the following.

The intersection of an infinite line in the *z* direction through x_{Can}, y_{Can}, i.e. the extended canister axis, with an infinite plane containing the generated fracture is determined. The equation of the plane can be written

$$(x - x_0)n_x + (y - y_0)n_y + (z - z_0)n_z = 0 \quad \text{(B-15)}$$

Inserting $x = x_{Can}$ and $y = y_{Can}$ yields

$$z_{Intersect} = z_0 - \frac{n_x}{n_z}(x_{Can} - x_0) - \frac{n_y}{n_z}(y_{Can} - y_0) \quad \text{(B-16)}$$

The intersection of the plane and an infinite vertical cylinder with axis through (x_{Can}, y_{Can}) takes the form of an ellipse with centre point (x_{Can}, y_{Can}, $z_{Intersect}$). In a co-ordinate system $(\hat{x}, \hat{y}, \hat{z})$ with the origin translated to this point, the equation of the plane can be written

$$\hat{x}n_x + \hat{y}n_y + \hat{z}n_z = 0 \quad \text{(B-17)}$$

and that of the infinite cylinder

$$\hat{x}^2 + \hat{y}^2 = r_{Can}^2 \quad \text{(B-18)}$$

Combining Equation (B-17) with Equation (B-18) yields the equation of the intersection ellipse as

$$n_x^2\left(r_{Can}^2 - \hat{y}^2\right) = \left(n_y\hat{y} + n_z\hat{z}\right)^2 \quad \text{(B-19)}$$

Solving this quadratic equation in $\hat{z}$ yields

$$\hat{z} = -\frac{n_y}{n_z}\hat{y} \pm \frac{n_x}{n_z}\sqrt{r_{Can}^2 - \hat{y}^2} \tag{B-20}$$

The max and min values of $\hat{z}$ are obtained through differentiation of $\hat{z}$ with respect to $\hat{y}$

$$\frac{d\hat{z}}{d\hat{y}} = -\frac{n_y}{n_z} \pm \frac{n_x}{n_z}\frac{-\hat{y}}{\sqrt{r_{Can}^2 - \hat{y}^2}} \tag{B-21}$$

The requirement

$$\frac{d\hat{z}}{d\hat{y}} = 0 \tag{B-22}$$

yields

$$\hat{y}^2\left[1 + \left(\frac{n_x}{n_y}\right)^2\right] = r_{Can}^2 \tag{B-23}$$

Inserting this result into Equation (B-20) yields

$$\hat{z}_{Max} = r_{Can}\frac{\sqrt{n_x^2 + n_y^2}}{|n_z|} \tag{B-24}$$

and

$$\hat{z}_{Min} = -r_{Can}\frac{\sqrt{n_x^2 + n_y^2}}{|n_z|} \tag{B-25}$$

In the original co-ordinate system, the minimum and maximum z-coordinates of the intersection ellipse are thus

$$z_{Max} = z_{Intersect} + r_{Can}\frac{\sqrt{n_x^2 + n_y^2}}{|n_z|} \tag{B-26}$$

and

$$z_{Min} = z_{Intersect} - r_{Can}\frac{\sqrt{n_x^2 + n_y^2}}{|n_z|} \tag{B-27}$$

respectively.

For a canister intersection to occur, it is necessary that

$$z_{Max} > -\frac{h_{Can}}{2} \tag{B-28}$$

and

$$z_{Min} < \frac{h_{Can}}{2} \tag{B-29}$$

In addition, the condition expressed by Equation (B-14) must be fulfilled.

Normalisation

In order to calculate the actual number of canister positions intersected by discriminating fractures, the actual density of fractures in the rock must be taken into account. In a rock volume V, the actual number of fractures, NF, with radii in the interval $[r_{Min}, r_{Max}]$ is

$$NF = V \int_{r_{Min}}^{r_{Max}} P_{32} \frac{(k-2) r_0^{k-2}}{\pi r^{k+1}} dr = V P_{32} \frac{(k-2) r_0^{k-2}}{k\pi} \left(\frac{1}{r_{Min}^k} - \frac{1}{r_{Max}^k} \right) \tag{B-30}$$

Enhancing the sampling efficiency

To obtain a more efficient sampling strategy, the scheme described below can be followed.

The volume, V, required to host all potentially discriminating fractures in a simulation is given by Equation (B-1). This volume is however required only for fractures of the maximum size r_{Max}. Since most of the generated fractures will typically be much smaller than r_{Max}, the majority of the simulated fractures will not give any canister intersections when distributed over the entire volume V.

The situation can be improved by observing that for smaller fractures, of radius r, only those located in the volume

$$V_r = (x_{Max} - x_{Min} + 2r)(y_{Max} - y_{Min} + 2r)(z_{Max} - z_{Min} + 2r)$$

$$= 8\left(r + \frac{x_{Max} - x_{Min}}{2} \right)\left(r + \frac{y_{Max} - y_{Min}}{2} \right)\left(r + \frac{z_{Max} - z_{Min}}{2} \right) \tag{B-31}$$

need to be considered as potentially jeopardising canister integrity. Therefore, fractures of size r can be generated in this smaller volume. This requires a modification of Equation (1) for the fracture size distribution in that Equation (1) must be multiplied by V_r/V yielding the modified distribution

$$f_1(r) = A\left(r^{2-k} + a_r r^{1-k} + b_r r^{-k} + c_r r^{-1-k} \right) \tag{B-32}$$

where A is a nomalisation constant. Denoting

$$x_L = \frac{x_{Max} - x_{Min}}{2}$$

etc, one obtains

$$a_r = x_L + y_L + z_L \tag{B-33}$$

$$b_r = y_L z_L + z_L x_L + x_L y_L \tag{B-34}$$

and

$$c_r = x_L y_L z_L \tag{B-35}$$

By requiring that the distribution function $F_1(r)$ equals 0 for $r = r_{Min}$ and 1 for $r = r_{Max}$, it can be demonstrated that

$$A = \left[\frac{r_{Max}^{3-k} - r_{Min}^{3-k}}{3-k} + \frac{a_r\left(r_{Max}^{2-k} - r_{Min}^{2-k}\right)}{2-k} + \frac{b_r\left(r_{Max}^{1-k} - r_{Min}^{1-k}\right)}{1-k} + \frac{c_r\left(r_{Max}^{-k} - r_{Min}^{-k}\right)}{-k} \right]^{-1} \tag{B-36}$$

The modified size distribution function $f_1(r)$ cannot be solved for r, as was the case for the original function. Instead, the sampling of r is obtained from a numerically pre-calculated distribution of r.

In the simulation, fractures of size r are thus generated only within the restricted volume V_r. In order to obtain a correct statistical distribution of fractures, also those outside this volume but within the larger volume V must be taken into account. One fracture within V_r corresponds to $(V - V_r)/V_r$ fractures of this nature. These latter are therefore registered in each realisation, see below.

The simulation is carried out according to the following:

- A fracture size, r, is sampled from the modified size distribution $f_1(r)$.
- The fracture location is sampled within the restricted volume V_r.
- The fracture orientation is determined as in the original scheme.
- The canister intersection tests are carried out as in the original scheme.
- A number of fractures of size r with centre points outside V_r but within V is recorded in order to obtain a correct statistical distribution. This number of non-intersecting fractures is $(V - V_r)/V_r$.

This modified scheme enhances the calculation efficiency by roughly a factor of 100.